




# *In vivo* Hyperpolarized Metabolic Imaging to Monitor the Progression of Hepatitis B Virus (HBV)-Related Hepatitis to Liver Fibrosis

Chung Man Moon<sup>1</sup> · Suk Hee Heo<sup>2,3</sup> · Yong Yeon Jeong<sup>2,3</sup> · Yun Young Lee<sup>3,4</sup> · Seul Kee Kim<sup>2,3</sup> · Sang Soo Shin<sup>3,4</sup> 

Received: 5 March 2024 / Revised: 25 June 2024 / Accepted: 1 July 2024 / Published online: 11 July 2024  
© The Author(s), under exclusive licence to World Molecular Imaging Society 2024

## Abstract

**Purpose** This study aimed to assess metabolic changes to monitor the progression from normal liver to hepatitis B virus (HBV)-related hepatitis and liver fibrosis using hyperpolarized <sup>13</sup>C magnetic resonance imaging (MRI).

**Procedures** Hepatitis was induced in mice (n = 16) via hydrodynamic injection of HBV 1.2 plasmid (25 µg). Among them, liver fibrosis was induced in the mice (n = 8) through weight-adapted administration of thioacetamide with ethanol. Normal control mice (n = 8) were injected with a phosphate buffer solution. Subsequently, a hyperpolarized <sup>13</sup>C MRI was performed on the mouse liver *in vivo*. The level of hepatitis B surface antigen (HBsAg) in blood serum was measured. Statistical analysis involved comparing the differential metabolite ratios, blood biochemistry values, and body weight among the three groups using the Kruskal–Wallis one-way analysis of variance.

**Results** HBsAg was absent in the normal and fibrosis groups, while it was detected in the hepatitis group. The ratios of [<sup>1-13</sup>C] lactate/pyruvate, [<sup>1-13</sup>C] alanine/pyruvate, [<sup>1-13</sup>C] lactate/total carbon, and [<sup>1-13</sup>C] alanine/total carbon were significantly lower in the normal control group than in the hepatitis and fibrosis groups (p < 0.05). Moreover, these ratios were significantly higher in the fibrosis group than in the hepatitis group (p < 0.05). However, no significant differences were observed in either [<sup>1-13</sup>C] pyruvate-hydrate/pyruvate or [<sup>1-13</sup>C] pyruvate-hydrate/total carbon among the three groups.

**Conclusions** The levels of [<sup>1-13</sup>C] lactate and [<sup>1-13</sup>C] alanine *in vivo* may serve as valuable indicators for differentiating between HBV-related hepatitis, liver fibrosis, and normal liver.

**Keywords** Hepatitis B virus · Acute hepatitis · Fibrosis · Hyperpolarization · <sup>13</sup>C magnetic resonance imaging

## Introduction

Hepatitis B virus (HBV) infection presents a significant global public health concern, with a prevalence rate of 3.5% observed worldwide [1, 2]. Moreover, chronic HBV infection tends to manifest asymptotically. Consequently, patients with chronic HBV face a significantly elevated risk of developing progressive fibrosis and liver cirrhosis if not promptly detected and actively monitored [3].

Chronic hepatitis B-related fibrosis has been specifically recognized as the hallmark indicator of the progression from mild hepatitis to marked liver dysfunction characterized by functional and structural abnormalities. This progression is characterized by hepatic sinusoidal capillarization and fibrosis in intrahepatic lobules and portal areas. These changes significantly affect the quality of life and health status of patients [4]. Moreover, research findings suggest that liver fibrosis can be reversed in patients with varying degrees of fibrosis by addressing underlying factors such as alcoholism

Chung Man Moon and Suk Hee Heo contributed equally to this work.

✉ Seul Kee Kim  
kimsk.rad@gmail.com

✉ Sang Soo Shin  
kjrads@gmail.com

<sup>1</sup> Research Institute of Medical Sciences, Chonnam National University, 264 Seoyang-ro, Hwasun-eup, Hwasun-gun, Jeollanam-do 58128, Republic of Korea

<sup>2</sup> Department of Radiology, Chonnam National University Hwasun Hospital, 322 Seoyang-ro, Hwasun-eup, Hwasun-gun, Jeollanam-do 58128, Republic of Korea

<sup>3</sup> Department of Radiology, Chonnam National University Medical School, 42 Jebong-ro, Dong-gu, Gwangju 61469, Republic of Korea

<sup>4</sup> Department of Radiology, Chonnam National University Hospital, 42 Jebong-ro, Dong-gu, Gwangju 61469, Republic of Korea

and HBV infection [5]. Early detection of hepatic fibrosis and timely provision of effective treatment would greatly benefit the patients by preventing disease progression. Hence, prioritizing effective measures for early diagnosis of liver fibrosis is essential in mitigating disease progression resulting from HBV infection.

Presently, the causes of liver fibrosis in patients with HBV and the mechanism underlying hepatitis B-related fibrosis remain incompletely understood [6]. Given the vital role of the liver as a metabolic organ, most hepatic injuries result in hepatocyte damage and disrupt cellular metabolism. Therefore, accurately assessing the status and monitoring dynamic changes of metabolic parameters in hepatitis and hepatic fibrosis is crucial for determining the appropriate treatment strategy to prevent hepatic fibrosis progression.

In clinical practice, routinely assessing liver fibrosis is crucial in patients with chronic hepatitis B infection [7]. Although histopathological assessment of hepatic tissues obtained from biopsy or hepatic resection remains the gold standard, these invasive techniques raise major concerns, including sampling error and potential complications. Thus, these procedures are less suitable for longitudinal follow-up [8]. Among noninvasive magnetic resonance imaging (MRI) techniques, hyperpolarized MRI utilizing carbon-13 ( $^{13}\text{C}$ ) labeled substrates enables real-time tracking of metabolic uptake and conversion *in vivo* within seconds. This approach provides unique metabolic insight into pathway-specific alterations without using ionizing radiation [9]. Hyperpolarized [1- $^{13}\text{C}$ ] pyruvate is currently the only probe available for human examinations. It has proven highly effective in investigating metabolic changes associated with early and precise diagnosis of liver disease, as well as in evaluating disease progression [9].

To date, four major types of HBV mouse models have been widely studied. These include the HBV transgenic mouse, human liver chimeric mouse, transduction of HBV replicons using adeno-associated virus, and hydrodynamic transduction of HBV replicons [10]. Moreover, a previous study [11] shows that a thioacetamide (TAA)-treated mouse model exhibited higher noticeable regenerative nodules, leading to the rapid formation of periportal fibrosis and, ultimately, cirrhosis. In conjunction with TAA, prolonged ethanol (EtOH) consumption can result in advanced hepatic impairment, such as simple steatosis, progressive fibrosis, and cirrhosis. Furthermore, repeated intraperitoneal injections of both TAA and EtOH have proven effective in inducing liver fibrosis in mice [12]. However, to our knowledge, no animal study has been reported to date that could differentiate between hepatitis and hepatic fibrosis.

Therefore, this study aimed to investigate the feasibility of using *in vivo* hyperpolarized  $^{13}\text{C}$  MRI to assess metabolite changes for monitoring the progression from acute hepatitis to liver fibrosis relative to a normal liver.

## Materials and Methods

### Animal Model

The Chonnam National University Medical School Research Institutional Animal Care and Use Committee approved the experimental protocol employed in this study. We utilized five-week-old C3H/HeN, pathogen-free, female mice ( $n = 24$ ; body weight, 18–20 g) obtained from Jungang Lab Animal, Inc., Korea, for all experiments.

Following 1 week of adaptation, hepatitis was induced in the mice ( $n = 16$ ) with a hydrodynamic injection of 25  $\mu\text{g}$  of HBV 1.2 plasmid via the tail vein, using a saline solution volume equivalent to 10% of the body weight of the mouse [10]. Among them, liver fibrosis was induced in the mice ( $n = 8$ ) through the weight-adapted administration of TAA solubilized in saline via the intraperitoneal route three times per week. Additionally, ethanol was orally administered through drinking water after weekly monitoring of the weight and health of each mouse for 12 weeks [11]. To minimize the effect of ethanol metabolism, ethanol intake was discontinued 1 week before hyperpolarized  $^{13}\text{C}$  MRI. Another group of mice ( $n = 8$ ) were injected with phosphate buffer solution (PBS, pH 7.4) as a normal control for 12 weeks, representing the mouse group without any treatment. Finally, mice were divided into three different groups: control ( $n = 8$ ), hepatitis ( $n = 8$ ), and liver fibrosis ( $n = 8$ ). After the  $^{13}\text{C}$  MRI examination,  $\text{CO}_2$  was employed as the euthanasia agent, and the mice were sacrificed at 12 weeks from baseline. Subsequently, blood was collected using the cardiac puncture method.

### Animal Preparation

In conducting  $^{13}\text{C}$  MRI, the mice were anesthetized with 2.5–4% isoflurane, along with oxygen (1 L/min). Subsequently, a catheter was inserted into the tail vein for the intravenous administration of the hyperpolarized [1- $^{13}\text{C}$ ] pyruvate solution. Simultaneously, the breathing rate was monitored throughout the data acquisition using a device (Model 1025; SA Instruments Inc., Stony Brook, NY, USA). The body temperature, measured with a rectal thermometer, was maintained between 36 °C and 37 °C via a flow of warm-water supply system.

### Polarization and Hyperpolarized $^{13}\text{C}$ Magnetic Resonance Imaging

As described in our previous papers [13–16], [1- $^{13}\text{C}$ ] pyruvic acid (25  $\mu\text{L}$ ; Isotec, Miamisburg, OH), doped with a 15 mM OX063 trityl radical (Oxford Instruments, Abingdon,

UK), was hyperpolarized using the HyperSense commercial polarizer (Oxford Instruments). The process involved 94.1 GHz irradiation in a 3.35 T field at 1.4 K for approximately 1 h. The hyperpolarized pyruvic acid sample was dissolved in 4 mL of an alkaline buffer, including 50 mM/L NaCl, 80 mM/L NaOH, 2.69 mM/L disodium EDTA, and 40 mM/L Trizma pre-set crystals, with a pH of 7.6. The resulting solution, with a concentration of 80 mM/L, was rapidly injected into the tail vein of mice that had undergone fasting for 12 h.

Hyperpolarized  $^{13}\text{C}$  MRI was performed using a 3 Tesla clinical MRI scanner (Discovery MR750; GE Healthcare, Milwaukee, WI, USA) equipped with a  $^1\text{H}/^{13}\text{C}$  dual mouse coil (Rapid Biomedical, Würzburg, Germany). A dynamic  $^{13}\text{C}$  magnetic resonance spectroscopy (MRS) study was conducted on liver tissue, with  $^{13}\text{C}$  spectra acquired every 2 s for 60 s immediately after injecting pyruvate (0.35 mL) from a 5.5-mm slice including most of the liver using a free induction decay chemical shift imaging (FIDCSI) pulse, featuring a slice-selective radiofrequency pulse with a  $10^\circ$  flip angle, 5000 Hz acquisition bandwidth, and 4096 points. Subsequently,  $^{13}\text{C}$  two-dimensional (2D) spectroscopic metabolic images were obtained 25 s after the injection of 0.35 mL pyruvate solution within 15 s. The imaging parameters included a field of view of  $50 \times 50 \text{ mm}^2$  in a 5.5-mm axial slice on the liver, matrix size of  $13 \times 13$ , and repetition time of 80 ms [15].

### Hyperpolarized $^{13}\text{C}$ spectral data processing

The  $^{13}\text{C}$  MR spectra underwent post-processing using SAGE software (GE Healthcare). They were apodized with a 9 Hz Gaussian filter and zero-filled to 16,384 data points. Following phase correction, the  $^{13}\text{C}$  MR spectra were analyzed. The following four major liver metabolites were assigned: [ $1\text{-}^{13}\text{C}$ ] lactate (185 ppm), [ $1\text{-}^{13}\text{C}$ ] pyruvate-hydrate (181 ppm), [ $1\text{-}^{13}\text{C}$ ] alanine (177 ppm), and [ $1\text{-}^{13}\text{C}$ ] pyruvate (172 ppm). Peak heights were used for quantifying each metabolite, yielding ratios of [ $1\text{-}^{13}\text{C}$ ] metabolite signals as relative values to the pyruvate peak and total carbon (tC) summed from all peak heights. This included lactate/pyruvate, lactate/tC, alanine/pyruvate, alanine/tC, pyruvate-hydrate/pyruvate, and pyruvate-hydrate/tC. Furthermore, the  $^{13}\text{C}$  2D metabolic imaging data underwent post-processing using Spectroscopic Image Visualization and Computing (SIVIC) software [17], with a 9 Hz Gaussian apodization, and were aligned with liver anatomic images. Color-coded maps were subsequently generated using a sinc-based interpolation to represent individual  $^{13}\text{C}$  metabolic imaging.

To assess the signal-to-noise ratio (SNR) for [ $1\text{-}^{13}\text{C}$ ] pyruvate, we calculated the ratio of its signal magnitude to the standard deviation of the noise in a region of the spectrum containing no signal [18].

### Blood Biochemistry

After the  $^{13}\text{C}$  MRI examination, mice were sacrificed, and the collected blood samples were centrifuged at 3,500 rpm for 15 min. The level of hepatitis B surface antigen (HBsAg) in blood serum, serving as a biomarker for HBV infection, was assessed using an enzyme-linked immunosorbent assay (ELISA; InTec Products, INC, China) with a colorimetric analysis and quantification method. Additionally, alanine aminotransferase (ALT), aspartate aminotransferase (AST), lactate dehydrogenase (LDH), alkaline phosphatase (ALP), creatine kinase (CK), blood urea nitrogen (BUN), and total protein (TP) were measured from blood serum samples using a blood chemistry analyzer (VET TEST 8008; IDEXX Laboratories, Westbrook, ME, USA).

### Histopathological Analysis

Mouse livers were extracted and fixed in 10% formalin. Based on the standard procedure outlined in a previous study [15], all the liver tissue fragments were embedded in paraffin and stained with hematoxylin–eosin (H&E) and Masson's trichrome (MT) by a single pathologist to assess HBV infection and hepatic fibrosis. The Batts–Ludwig classification system [19] was used to evaluate the degree of fibrosis, categorized as follows: stage 0 (no fibrosis), stage 1 (portal fibrosis, fibrous portal expansion), stage 2 (periportal or portal-portal septa), stage 3 (septal fibrosis, fibrous septa with architectural distortion; no obvious cirrhosis), and stage 4 (cirrhosis).

### Statistical Analysis

Statistical analyses were performed using MedCalc software version 19.0.4 (MedCalc Software, Ostend, Belgium) and SPSS 24.0 software (SPSS Inc., Chicago, IL). The data were analyzed using the Kruskal–Wallis one-way analysis of variance with a post hoc test at  $p < 0.05$  to compare the differential metabolite ratios, blood biochemistry values, and body weight among the three groups.

## Results

### Body Weight

The body weight of the mice did not show significant differences among the three groups (normal control vs. hepatitis vs. fibrosis =  $21.89 \pm 1.82 \text{ g}$  vs.  $20.71 \pm 1.85 \text{ g}$  vs.  $19.75 \pm 2.43 \text{ g}$ , respectively).



## Hepatic Histopathology

H&E staining of the liver tissue from the normal control mouse (Fig. 1a) revealed well-preserved hepatic cell plates and minimal inflammation at the portal triad, with no hepatitis and fibrosis observed on MT staining.

Compared to the normal control, Fig. 1b depicts a portal triad with minimal inflammatory cell infiltration but notably advanced viral cytopathic changes in HBV-infected mouse. Mildly disrupted hepatocyte plates comprised degenerating hepatocytes with swollen pale cytoplasm. However, fibrosis was not observed in MT staining, comparable to the normal control (Fig. 1b). In the hepatic fibrosis group (n=8), five mice were categorized as stage 1, while three were classified as stage 2 based on histopathological results. Figure 1c illustrates mild fibrosis restricted to portal areas (stage 1) or fibrosis extending to areas near the portal vein (stage 2).

## Blood Biochemistry

In the ELISA assay for HBsAg, HBsAg was absent in the normal control and fibrosis groups, while it was detected in the hepatitis group. This finding confirmed the effective transfection of the HBV 1.2 plasmid into the hepatocytes of the hepatitis group (Fig. 2).

Additionally, serum AST, LDH, ALP, BUN, TP, and CK levels did not differ significantly among the three groups (Fig. 2). However, only the ALT level in the hepatitis and fibrosis groups was increased than that in the normal control group.

## *In vivo* $^{13}\text{C}$ MR Spectroscopy and Imaging

Figure 3 displays anatomical MRI image of the liver (Fig. 3a), stacked spectra (Fig. 3b) and the average spectra (Fig. 3c) reconstructed from the dynamic spectra covering 60 s. Dynamic intensity curves depict the time course of all [ $^{13}\text{C}$ ] metabolites (Fig. 3d), while metabolite-to-pyruvate ratios (Fig. 3e) demonstrate that lactate and alanine concentrations gradually increased upon pyruvate injection. Figure 3f shows all integral curves of [ $^{13}\text{C}$ ] metabolites over the time course.

The mean SNR of pyruvate was  $77.83 \pm 11.64$  in the normal liver,  $70.63 \pm 10.21$  in hepatitis liver, and  $67.93 \pm 10.16$  in fibrosis liver, with no statistically significant difference among the groups ( $p=0.20$ ).

The ratios of [ $^{13}\text{C}$ ] lactate/pyruvate, [ $^{13}\text{C}$ ] alanine/pyruvate, [ $^{13}\text{C}$ ] lactate/tC, and [ $^{13}\text{C}$ ] alanine/tC were significantly lower in the normal control group than in the hepatitis and fibrosis groups ( $p < 0.05$ ) (Fig. 4). Moreover, these ratios were significantly higher in the fibrosis group

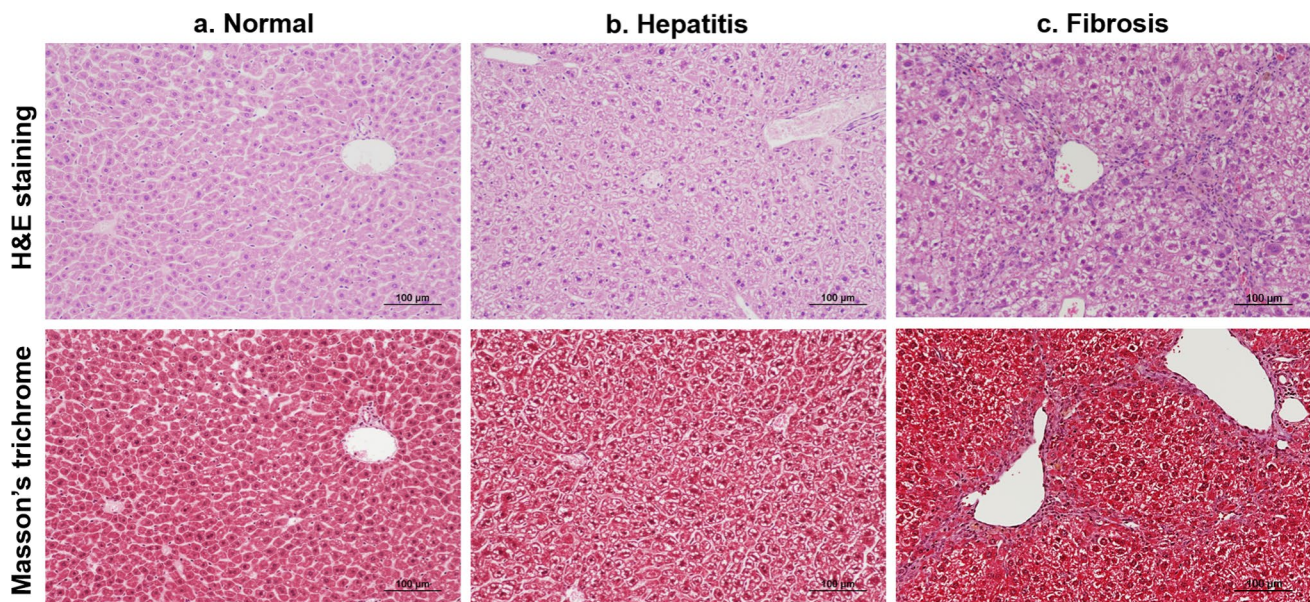


**Fig. 1** Representative hepatic histopathology stained with hematoxylin and eosin (H&E) and Masson's trichrome (MT). (a) H&E-stained liver tissue from a normal control mouse shows well-preserved hepatic cell plates with minimal inflammation at the portal triad. No signs of hepatitis or fibrosis are observed, as confirmed by MT staining. (b) H&E-stained liver tissue from an HBV-infected mouse reveals minimal inflammatory cell infiltration at the portal triad and

advanced viral cytopathic changes. The hepatocyte plates appear mildly disrupted, with degenerating hepatocytes exhibiting swollen, pale cytoplasm. MT staining shows no evidence of fibrosis, similar to the normal control. (c) Liver tissue from a mouse in the hepatic fibrosis group shows fibrosis extending to areas near the portal vein. Bar = 100 µm.

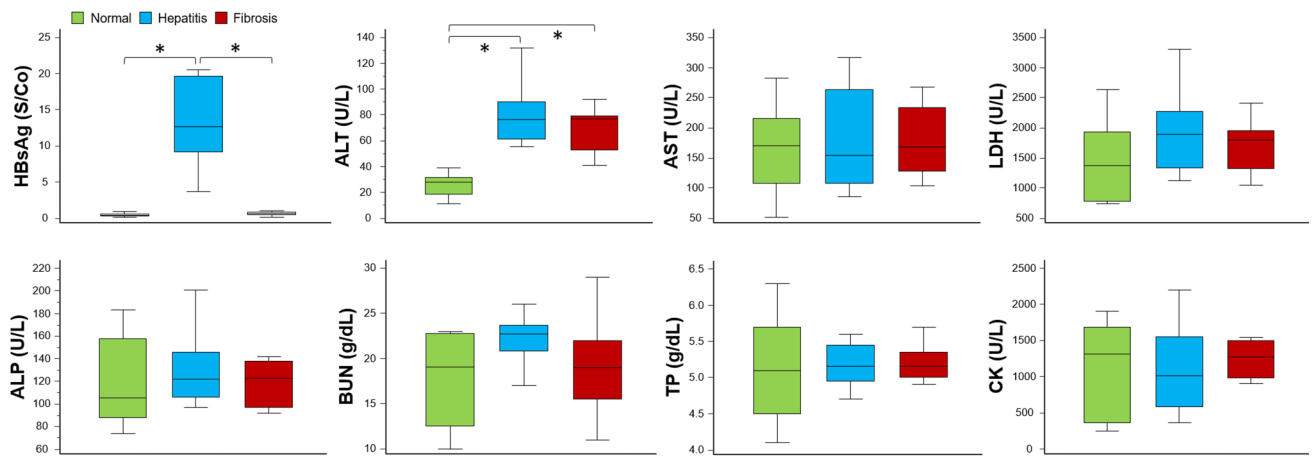


**Fig. 2** Blood chemistry results among the normal, hepatitis, and fibrosis groups. HBsAg was detected only in the hepatitis group, confirming HBV plasmid transfection. ALT levels were significantly elevated in the hepatitis and fibrosis groups compared to the normal group. No significant differences were observed in AST, LDH, ALP, BUN, TP, and CK levels among the three groups. HBsAg, hepatitis

B surface antigen; S/Co, signal-to-cutoff ratio; ALT, alanine aminotransferase; AST, aspartate aminotransferase; LDH, lactate dehydrogenase; ALP, alkaline phosphatase; BUN, blood urea nitrogen; TP, total protein; and CK, creatine kinase. \* indicates a significant difference among the three groups via the Kruskal–Wallis one-way analysis of variance with a post hoc test at  $p < 0.05$ .

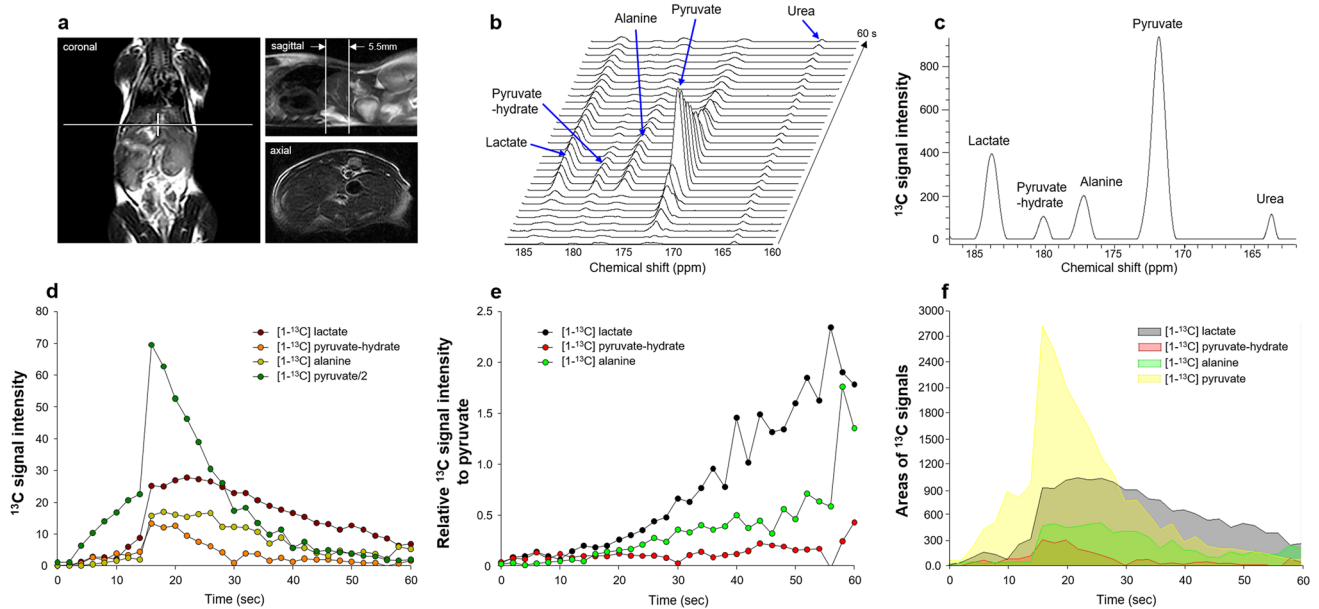
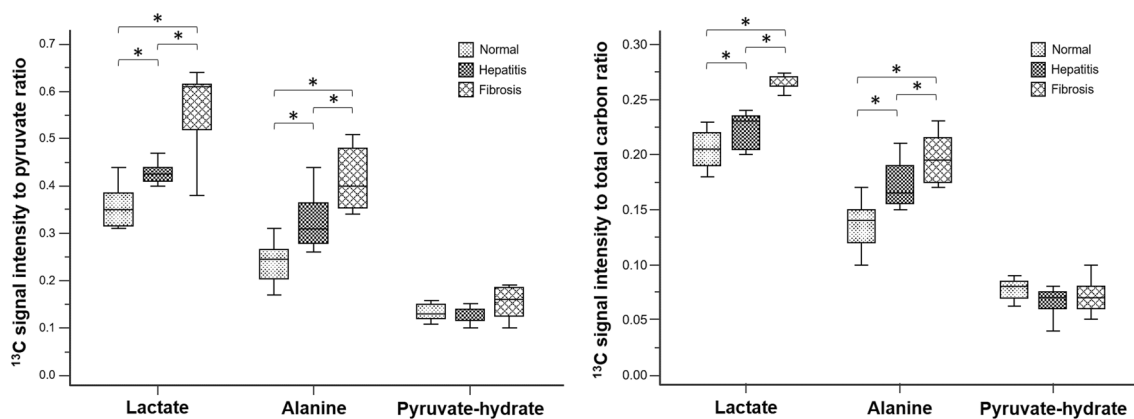


**Fig. 3** (a) Anatomical MRI image of the liver, showing detailed liver structure and position for subsequent hyperpolarized  $^{13}\text{C}$  magnetic resonance spectroscopic imaging. (b) Stacked spectra of hyperpolarized  $[1-^{13}\text{C}]$  metabolites, illustrating the individual spectra acquired over the 60-s observation period. Each spectrum is plotted over time to demonstrate the dynamic changes in metabolite signals. (c) Average spectra from the dynamic spectra covering 60 s. (d) Dynamic

intensity curves showing the time course of each  $[1-^{13}\text{C}]$  metabolite. (e) Metabolite-to-pyruvate ratios over the time course. These ratios depict the relative concentrations of lactate, pyruvate-hydrate, and alanine compared to pyruvate, showing the metabolic conversion dynamics and how the concentrations of these metabolites gradually increase upon pyruvate injection. (f) Integral curves showing the integrated signal of each  $[1-^{13}\text{C}]$  metabolite over the time course.

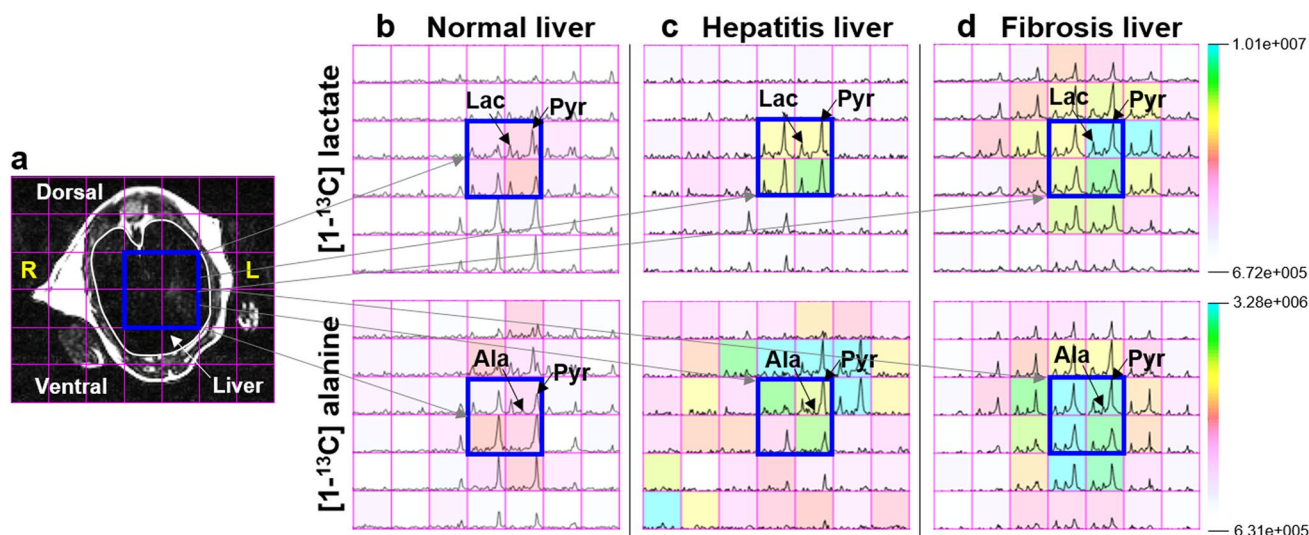
than in the hepatitis group ( $p < 0.05$ ). However, no significant differences were observed in either  $[1-^{13}\text{C}]$  pyruvate-hydrate/pyruvate or  $[1-^{13}\text{C}]$  pyruvate-hydrate/tC among the three groups.

Figure 5 displays  $^{13}\text{C}$  spectroscopic imaging of hyperpolarized  $[1-^{13}\text{C}]$  lactate and  $[1-^{13}\text{C}]$  alanine signals in each group. The metabolic maps derived from pyruvate show a similar pattern consistent with the results obtained from  $^{13}\text{C}$



**Fig. 4** Changes in  $^{13}\text{C}$ -labeled metabolite ratios across normal, hepatitis, and fibrosis groups. These ratios are significantly lower in the normal group compared to the hepatitis and fibrosis groups and higher in the fibrosis group compared to the hepatitis group. No sig-

nificant differences are noted for  $[1-^{13}\text{C}]$  pyruvate-hydrate/pyruvate or  $[1-^{13}\text{C}]$  pyruvate-hydrate/tC among the groups. \* indicates a significant difference among the three groups using the Kruskal–Wallis one-way analysis of variance with a post hoc test at  $p < 0.05$ .



**Fig. 5** Representative hyperpolarized  $^{13}\text{C}$  magnetic resonance spectroscopic imaging data, showing (a) axial T2-weighted image of the liver. The corresponding  $^{13}\text{C}$  magnetic resonance spectra of  $[1-^{13}\text{C}]$  lactate (Lac) and  $[1-^{13}\text{C}]$  alanine (Ala) in (b) normal, (c) hepatitis, and (d) fibrosis livers. Each spectroscopic voxel exhibits signals from the injected substrate, pyruvate (Pyr, 172 ppm), and its meta-

bolic products, Lac (185 ppm) and Ala (177 ppm). Colormap overlay images show a similar pattern consistent with the results obtained from  $^{13}\text{C}$  dynamic MRS, indicating higher  $[1-^{13}\text{C}]$  Lac/Pyr and  $[1-^{13}\text{C}]$  Ala/Pyr ratios in fibrosis liver, reflecting significant metabolic changes compared to normal and hepatitis livers. R: right, L: left.

dynamic MRS, indicating higher ratios of  $[1-^{13}\text{C}]$  lactate/pyruvate and  $[1-^{13}\text{C}]$  alanine/pyruvate in the fibrosis group than in other groups.

## Discussion

While the pathological processes resulting from HBV infection and fibrosis have been extensively described, there remains limited detailed comprehension of the distinct

features of dynamic hepatic metabolism transitioning from hepatitis to fibrosis. This limitation is primarily attributed to the lack of suitable *in vivo* infection models [20]. Therefore, this study aimed to assess the real-time dynamic changes in cellular metabolites, progressing from HBV infection in a mouse model to liver fibrosis. This assessment was conducted utilizing *in vivo* hyperpolarized dynamic  $^{13}\text{C}$  MRS, which provides high spectral resolution and enables metabolic imaging. We successfully induced hepatitis and fibrosis models in mice by employing HBV infection and TAA/EtOH



injection, respectively, based on methodologies described in previous studies [10, 11]. Compared to normal control mice, hepatitis and fibrosis mice exhibited significant alterations in blood biochemical and histopathological results. A previous study [10] revealed elevated levels of serum ALT, AST, and LDH in hepatitis and fibrosis mice, suggesting a potential association with hepatic parenchymal injury and/or cell necrosis. In the histopathological findings, infiltration of inflammatory cells was observed in portal tracts surrounding HBsAg-positive hepatocytes in the HBV group. Additionally, increased inflammatory infiltration was observed in the portal and central areas, along with linear bridging fibrosis in the fibrosis group.

This preclinical study on liver metabolism in hepatitis and liver fibrosis serves to bridge the translational gap of hyperpolarized  $^{13}\text{C}$  MRI. Moreover, it offers fundamental insight that may aid in predicting clinical outcomes for patients with liver diseases. Real-time visualization of specific metabolic markers, such as  $[1-^{13}\text{C}]$  lactate and  $[1-^{13}\text{C}]$  alanine, provides valuable insight into intracellular metabolism. These markers can be used noninvasively to monitor disease progression and treatment response.

While previous studies [13–15, 21] using hyperpolarized  $^{13}\text{C}$  MRI have indicated an association between the conversion rate of  $[1-^{13}\text{C}]$  pyruvate to  $[1-^{13}\text{C}]$  lactate and  $[1-^{13}\text{C}]$  alanine and abnormal glucose metabolism in the hepatic biochemical pathway, significant alterations in cellular metabolite levels during the progression from hepatitis to hepatic fibrosis remain unidentified. In this study, the levels of  $[1-^{13}\text{C}]$  lactate and  $[1-^{13}\text{C}]$  alanine exhibited a significant increase in the hepatitis and fibrosis groups than in the control group. This outcome may be attributed to altered glycolysis and gluconeogenesis activity within liver metabolism stimulated by hepatitis B infection, eventually leading to hepatic fibrosis.

It remains unclear whether lactate—considered the main end product of anaerobic metabolism—can reliably predict the prognosis of patients with HBV infection [22, 23]. HBV specifically targets hepatocytes, increasing the glycolytic activity within infected cells [24]. Moreover, cells utilize carbohydrates, especially glucose, which undergoes glycolysis to generate pyruvate, thereby producing adenosine triphosphate and other precursors for various metabolic pathways [25]. Heightened glycolytic activity correlates with a decrease in oxidative phosphorylation, leading to the conversion of pyruvate to lactate, thus promoting the flow of glycolytic intermediates necessary for anaplerosis [25]. Additionally, HBV infection is known to activate the pentose phosphate pathway, thereby supplying substrates for nucleotide synthesis crucial for HBV replication through metabolic reprogramming [26]. In summary, HBV appears to reprogram cellular glucose metabolism, potentially contributing to the development of HBV-associated hepatic fibrosis.

A metabolomic study [27] exploring biochemical alteration in liver tissue and serum in a rat model of experimentally induced fibrosis and cirrhosis revealed elevated levels of lactate in serum. This outcome is attributed to glycogenolysis, glycolysis, and a degree of anaerobic metabolism within the fibrotic liver, as previously observed in acute liver injury [28]. Moreover, the rise in plasma lactate is suggested to correspond with a shift in energy metabolism towards ketone body formation [27]. Owing to dysregulated glucose metabolism, the elevated lactate levels could reflect hepatic HBV infection and fibrosis development in liver tissue, possibly disrupting key metabolic pathways.

Alanine plays a crucial role in the uptake and catabolism of amino acids for hepatic gluconeogenesis [29]. Moreover, the interconversion of alanine-pyruvate is facilitated by the ALT enzyme, which is abundant in the cytoplasm of hepatocytes—a liver metabolite [30]. When hepatocytes are damaged, ALT is released into the serum from injured hepatocytes, resulting in an increase in serum ALT activity [31]. Based on a previous study [32], in an acute hepatocyte injury model induced via chemical hepatotoxicity, the alanine/tC ratio and ALT level were significantly increased than those in normal liver. They suggested that  $[1-^{13}\text{C}]$  alanine could serve as a noninvasive and sensitive biomarker for liver diseases across various histopathological states. Furthermore, a study [33] on amino acid composition revealed increased levels of branched-chain amino acids and other amino acids, including glutamate, glutamine, and alanine, in patients with liver fibrosis. Based on these studies, it could be hypothesized that hepatic injury induces alteration of ALT levels, consequently increasing alanine levels in hepatocytes. However, the exact pathophysiological role of alanine metabolite in liver disease progression remains unknown. Our findings are consistent with those of previous studies, which revealed that hepatic metabolic dysregulation is one of the signature features of HBV infection and fibrosis. Therefore, the  $[1-^{13}\text{C}]$  alanine level in hepatic parenchyma may potentially be related to the disruption of transamination in metabolic fluxes induced by hepatitis and fibrosis. Consequently, it could serve as a crucial quantitative biomarker for the early detection of hepatitis and liver fibrosis.

This study had some limitations. First, the sample size in each group was relatively small. Therefore, further longitudinal studies should include a larger number of mice to enhance statistical power and validate the metabolic changes associated with  $[1-^{13}\text{C}]$  pyruvate metabolism. Second, combining hyperpolarized  $^{13}\text{C}$  MRI with positron emission tomography may provide complementary insight and enhance our understanding of the biological processes in the progression from hepatitis to hepatic fibrosis. Thirdly, only  $^{13}\text{C}$ -labeled pyruvate was used as a substrate in this study. Hence, for future research endeavors, simultaneous co-polarization and/or co-injection of multiple compounds,

such as glutamine, ethyl acetoacetate, dehydroascorbic acid, and dihydroxyacetone could facilitate the evaluation of various cellular processes concurrently [9]. Lastly, we did not include experiments for measuring LDHA/B levels or monocarboxylate transporters, which correlate with lactate levels.

In conclusion, our results suggest that changes in hyperpolarized  $^{13}\text{C}$  metabolites may serve as effective biomarkers to distinguish between HBV-related hepatitis, liver fibrosis, and normal liver.

**Supplementary Information** The online version contains supplementary material available at <https://doi.org/10.1007/s11307-024-01936-8>.

**Author Contributions** Moon CM, Heo SH, Kim SK, and Shin SS designed the study; Moon CM, Heo SH, and Jeong YY performed the majority of experiments; Moon CM, Heo SH, Lee YY, and Shin SS contributed to the analysis and interpretation of results; Moon CM, and Heo SH wrote the first draft of the manuscript; Kim SK, and Shin SS have approved the final manuscript and completed manuscript; Also, all authors agree with the content of the manuscript.

**Funding** This study was financially supported by the Ministry of Science and ICT through the National Research Foundation of Korea (No. 2021R1A2C1005765; 2021H1D3A2A02037997; 2022R1A2C1003266; RS-2023-00245913; RS-2024-00333646).

**Data Availability** The datasets acquired from the current study are available from the corresponding author upon reasonable request.

## Declarations

**Ethical Approval** The Chonnam National University Medical School Research Institutional Animal Care and Use Committee approved the experimental protocol employed in this study.

**Conflict of Interest** The authors have no relevant financial or non-financial interests to disclose.

## References

1. Yuen MF, Chen DS, Dusheiko GM et al (2018) Hepatitis B virus infection. *Nat Rev Dis Primers* 4:18035
2. Jieanu CF, Ungureanu BS, Sandulescu DL et al (2015) Quantification of liver fibrosis in chronic hepatitis B virus infection. *J Med Life* 8:285–290
3. Chen J, Yu S, Lang Z et al (2023) Development and validation of a potential biomarker to improve the assessment of liver fibrosis progression in patients with chronic hepatitis B. *J Med Virol* 95:e28239
4. Wang C, Zheng L, Li Y et al (2022) Noninvasive Assessment of Liver Fibrosis and Inflammation in Chronic Hepatitis B: A Dual-task Convolutional Neural Network (DTCNN) Model Based on Ultrasound Shear Wave Elastography. *J Clin Transl Hepatol* 10:1077–1085
5. Liao MJ, Li J, Dang W et al (2022) Novel index for the prediction of significant liver fibrosis and cirrhosis in chronic hepatitis B patients in China. *World J Gastroenterol* 28:3503–3513
6. Yang J, Gu J, Wang H et al (2022) Fc receptor-like 5 gene polymorphisms and mRNA expression are associated with liver fibrosis in chronic hepatitis B. *Front Microbiol* 13:988464
7. Bui HH, Vo VH, Nguyen CD, Phan ST, Quach PT, Nguyen DB (2022) Diagnostic Performance of Acoustic Radiation Force Impulse Imaging in Evaluating Liver Fibrosis in Patients with Chronic Hepatitis B Infection: A Cross-Sectional Study. *Indian J Radiol Imaging* 32:287–293
8. Meng F, Zheng Y, Zhang Q et al (2015) Noninvasive evaluation of liver fibrosis using real-time tissue elastography and transient elastography (FibroScan). *J Ultrasound Med* 34:403–410
9. Ye Z, Song B, Lee PM, Ohliger MA, Laustsen C (2022) Hyperpolarized carbon 13 MRI in liver diseases: Recent advances and future opportunities. *Liver Int* 42:973–983
10. Poilil Surendran S, George Thomas R, Moon MJ et al (2020) Effect of hepato-toxins in the acceleration of hepatic fibrosis in hepatitis B mice. *PLoS ONE* 15:e0232619
11. Thomas RG, Moon MJ, Kim JH, Lee JH, Jeong YY (2015) Effectiveness of Losartan-Loaded Hyaluronic Acid (HA) Micelles for the Reduction of Advanced Hepatic Fibrosis in C3H/HeN Mice Model. *PLoS ONE* 10:e0145512
12. Kornek M, Raskopf E, Guetgemann I et al (2006) Combination of systemic thioacetamide (TAA) injections and ethanol feeding accelerates hepatic fibrosis in C3H/He mice and is associated with intrahepatic up regulation of MMP-2, VEGF and ICAM-1. *J Hepatol* 45:370–376
13. Moon CM, Oh CH, Ahn KY et al (2017) Metabolic biomarkers for non-alcoholic fatty liver disease induced by high-fat diet: *In vivo* magnetic resonance spectroscopy of hyperpolarized [1-(13)C] pyruvate. *Biochem Biophys Res Commun* 482:112–119
14. Moon CM, Shin SS, Lim NY et al (2018) Metabolic alterations in a rat model of hepatic ischaemia reperfusion injury: *In vivo* hyperpolarized (13) C MRS and metabolic imaging. *Liver Int* 38:1117–1127
15. Moon CM, Shin SS, Heo SH et al (2019) Metabolic Changes in Different Stages of Liver Fibrosis: *In vivo* Hyperpolarized (13) C MR Spectroscopy and Metabolic Imaging. *Mol Imaging Biol* 21:842–851
16. Moon CM, Kim YH, Ahn YK, Jeong MH, Jeong GW (2019) Metabolic alterations in acute myocardial ischemia-reperfusion injury and necrosis using *in vivo* hyperpolarized [1-(13)C] pyruvate MR spectroscopy. *Sci Rep* 9:18427
17. Crane JC, Olson MP, Nelson SJ (2013) SIVIC: Open-Source, Standards-Based Software for DICOM MR Spectroscopy Workflows. *Int J Biomed Imaging* 2013:169526
18. Nguyen NT, Rasanjala ONMD, Park I (2022) Optimization of Scan Parameters for *in vivo* Hyperpolarized Carbon-13 Magnetic Resonance Spectroscopic Imaging. *Investig Magn Reson Imaging* 26:125–134
19. Batts KP, Ludwig J (1995) Chronic hepatitis. An update on terminology and reporting. *Am J Surg Pathol* 19:1409–1417
20. Yu L, Zeng Z, Tan H et al (2022) Significant metabolic alterations in patients with hepatitis B virus replication observed via serum untargeted metabolomics shed new light on hepatitis B virus infection. *J Drug Target* 30:442–449
21. Darpolor MM, Yen YF, Chua MS et al (2011) *In vivo* MRSI of hyperpolarized [1-(13)C]pyruvate metabolism in rat hepatocellular carcinoma. *NMR Biomed* 24:506–513
22. Nie Y, Liu LX, Chen T, Zhang Y, Zhu X (2021) Serum lactate level predicts 6-months mortality in patients with hepatitis B virus-related decompensated cirrhosis: a retrospective study. *Epidemiol Infect* 149:e26
23. Doherty JR, Cleveland JL (2013) Targeting lactate metabolism for cancer therapeutics. *J Clin Invest* 123:3685–3692
24. Wan Q, Wang Y, Tang H (2017) Quantitative (13)C Traces of Glucose Fate in Hepatitis B Virus-Infected Hepatocytes. *Anal Chem* 89:3293–3299



25. Diaz O, Vidalain PO, Ramiere C, Lotteau V, Perrin-Cocon L (2022) What role for cellular metabolism in the control of hepatitis viruses? *Front Immunol* 13:1033314
26. Masson JJ, Billings HW, Palmer CS (2017) Metabolic reprogramming during hepatitis B disease progression offers novel diagnostic and therapeutic opportunities. *Antivir Chem Chemother* 25:53–57
27. Constantinou MA, Theocharis SE, Mikros E (2007) Application of metabonomics on an experimental model of fibrosis and cirrhosis induced by thioacetamide in rats. *Toxicol Appl Pharmacol* 218:11–19
28. Waters NJ, Waterfield CJ, Farrant RD, Holmes E, Nicholson JK (2005) Metabonomic deconvolution of embedded toxicity: application to thioacetamide hepato- and nephrotoxicity. *Chem Res Toxicol* 18:639–654
29. Brosnan JT, Brosnan ME, Yudkoff M et al (2001) Alanine metabolism in the perfused rat liver. Studies with (15)N. *J Biol Chem* 276:31876–31882
30. Lee DY, Kim EH (2019) Therapeutic Effects of Amino Acids in Liver Diseases: Current Studies and Future Perspectives. *J Cancer Prev* 24:72–78
31. KimFlammDiBisceglieBodenheimer WRSLAMHC, Public Policy Committee of the American Association for the Study of Liver D (2008) Serum activity of alanine aminotransferase (ALT) as an indicator of health and disease. *Hepatology* 47:1363–1370
32. Kim GW, Oh CH, Kim JC et al (2016) Noninvasive biomarkers for acute hepatotoxicity induced by 1,3-dichloro-2-propanol: hyperpolarized <sup>13</sup>C dynamic MR spectroscopy. *Magn Reson Imaging* 34:159–165
33. Hasegawa T, Iino C, Endo T et al (2020) Changed amino acids in NAFLD and liver fibrosis: a large cross-sectional study without influence of insulin resistance. *Nutrients* 12(5):1450

**Publisher's Note** Springer Nature remains neutral with regard to jurisdictional claims in published maps and institutional affiliations.

Springer Nature or its licensor (e.g. a society or other partner) holds exclusive rights to this article under a publishing agreement with the author(s) or other rightsholder(s); author self-archiving of the accepted manuscript version of this article is solely governed by the terms of such publishing agreement and applicable law.